

# First-order displacive structural phase transitions studied by computer simulation

W. C. Kerr and A. M. Hawthorne\*

*Olin Physical Laboratory, Wake Forest University, Winston-Salem, North Carolina 27109-7507*

R. J. Gooding

*Department of Physics, Queens University, Kingston, Ontario, Canada K7L 3N6*

A. R. Bishop

*Theoretical Division, Los Alamos National Laboratory, Los Alamos, New Mexico 87545*

J. A. Krumhansl

*Laboratory of Atomic and Solid State Physics, Cornell University, Ithaca, New York 14853*

(Received 12 September 1991)

We have constructed a lattice-dynamical model which possesses many of the features occurring at first-order structural phase transitions in solids. The model includes an asymmetric nonlinear on-site potential and anharmonic interparticle interactions. The anharmonicity in the interaction is introduced in a way which lowers the phonon frequencies in the high-temperature, metastable phase. The interaction provides a mechanism for a vibrational-entropy-driven first-order phase transition. We present results from molecular-dynamics calculations which show (i) clear evidence in the thermodynamic functions for the existence of a first-order phase transition produced by heating from low temperature, and (ii) unusual properties for the position probability distribution and the dynamic structure factor. These spectral functions have significant intensity in the quasielastic region, and this contribution is strongly maximized near the transition temperature. The wave-vector dependence of this "central peak" clearly points to the existence of propagating nonlinear modes.

## I. INTRODUCTION

This paper is concerned with understanding the microscopic character of a significant class of displacive phase transitions, particularly those involving body-centered-cubic ( $\beta$  cubic) to close-packed arrangements, which occur in, e.g., alkali metals and martensitic alloys. Over the past several years a large amount of accurate experimental information has been obtained (see, e.g., the recent summary of displacive transformations from  $\beta$  cubic to  $\alpha$  hcp, or  $\beta$  cubic to the  $\omega$  phase in pure Ti and Zr by Heiming *et al.*,<sup>1</sup> and references therein). These transformations are diffusionless, being accomplished specifically by a particular set of displacive distortions of the  $\beta$ -cubic lattice to produce a different symmetry structure. The transformations are *topologically* reversible, and the relationship between the high- and low-temperature structures is referred to as a lattice correspondence. In general, both elastic strains and modulation waves may be involved. A useful brief discussion of this structural relationship concept is found in Lindgård and Mouritsen<sup>2</sup> and more extensively in Nishiyama.<sup>3</sup>

The important heuristic advance in describing these transitions combined two ideas: employing a Landau expansion of the free energy in powers of the amplitudes of the distortion modes with the relevant symmetry *and* using mode frequencies which are temperature dependent due to lattice anharmonicity.<sup>4</sup> This free-energy function and the temperature-dependent quasi-harmonic mode frequencies derive from essentially mean-field approxima-

tions to the statistical mechanics. One of the early motivating examples was a theory of the ferroelectric transition described by a specific static displacement corresponding to an optical mode, e.g., of a perovskite lattice. For that transition, Cochran and Anderson postulated a free energy<sup>5,4</sup>

$$F = \frac{1}{2}a(T - T_0)\eta^2 + \frac{1}{4}B\eta^4 + \dots, \quad (1.1)$$

where  $\eta$  denotes the static, uniform displacement amplitude. For  $T > T_0$ , this polynomial form for  $F$  is minimized by  $\eta_s = 0$ , while for  $T < T_0$ ,  $F$  develops an unstable maximum at  $\eta = 0$  and stable minima at  $\eta_s = \pm[a|T - T_0|/B]^{1/2}$ . Thus, as  $T$  decreases through  $T_0$ ,  $\eta_s$  grows continuously from its zero value above  $T_0$ , proportionally to  $|T - T_0|^{1/2}$ . (As is well known, diverging fluctuations change the exponent from the mean-field value of  $\frac{1}{2}$ , but the values of the critical exponents are not of primary concern here.) Concurrently, there is a close relation between the coefficient of the  $\eta^2$  term and the quasi-harmonic frequency measured by inelastic neutron scattering:

$$m^* \omega_{\text{opt}}^2 \simeq a(T - T_0), \quad (1.2)$$

where  $m^*$  is an appropriate reduced mass. Though postulated by Cochran and by Anderson, formal demonstration of this relation was given by Cowley<sup>6</sup> and by Maradudin and Fein<sup>7</sup> using many-body anharmonic phonon perturbation theory. Equations (1.1) and (1.2) together give the "soft-mode" theory of displacive transitions.<sup>4</sup>

Its key features are (1) the lattice becomes unstable against static displacements in a particular mode when the quasiharmonic frequency of that mode goes to zero at  $T = T_0$ , (2) the resulting distortion of the lattice produces a new phase (the high- and low-temperature phases are known as parent and product phases, respectively), (3) the description is limited to second-order transitions since the order parameter  $\eta$  changes continuously at  $T_0$ .

This classic “soft-mode” theory, being both intuitively appealing and easy to apply to data, has been widely invoked and for a few prototypic materials has been remarkably successful, considering the level of approximation involved. However, the following observations showed that important features were missing from the theory: (1) the existence of the “central peak,” i.e., the anomalous, large quasielastic intensity in neutron-scattering experiments; (2) the fact that very few transforming materials showed the magnitude of “softening” needed to fit a soft-mode model; (3) evidence for precursor structures in many, but not all, cases. Indeed, precise experiments by Müller<sup>8</sup> on carefully prepared perovskite samples showed evidence for precursor regions of the product phase, even in the purest samples. Stimulated by these anomalies, research was initiated on model systems where the statistical mechanics could be treated exactly,<sup>9</sup> e.g., by the transfer integral method for the one-dimensional (1D) systems or by the Onsager method for highly anisotropic 2D systems. Increasing computational capabilities also motivated research on these model systems by molecular dynamics.<sup>10,11</sup>

The prototypic case of these model systems, the so-called “ $\phi^4$  model,” begins with an on-site potential energy (*not free energy*),

$$V(u_i) = -\frac{1}{2}\alpha u_i^2 + \frac{1}{4}\beta u_i^4, \quad (1.3)$$

where  $u_i$  is a one-component dynamical variable (a *displacement* in this lattice-dynamical context) at each lattice site  $i$ . In addition, displacements at nearest-neighbor sites are coupled harmonically,  $V(u_i, u_j) = v_{ij}(u_i - u_j)^2/2$ . The order parameter is the average displacement,  $\eta = \langle u_i \rangle$ , where  $\langle \dots \rangle$  denotes finite-temperature ensemble average. The potential  $V(u)$  has degenerate minima at  $\pm(\alpha/\beta)^{1/2}$ , and so the  $T=0$  ground state is a broken symmetry state with uniform displacements throughout the system, giving  $\eta = \pm(\alpha/\beta)^{1/2}$ . In contrast, at sufficiently high temperature,  $\eta=0$ . The simulations by Schneider and Stoll<sup>10</sup> and by Kerr and Bishop<sup>11</sup> bear out the expected behavior in 2D or 3D. Of the three experimental features listed above which are missing from the soft-mode model, the simulations<sup>10,11</sup> confirm the existence both of a central peak not related to impurities and of precursors, in accord with Müller’s<sup>8</sup> experiments. A soft mode, which displays a substantial decrease in frequency as  $T$  changes, is present in these computer simulations, but, as discussed by Kerr and Bishop,<sup>11</sup> there are important additional features beyond the original soft-mode theory.

The  $\phi^4$  model still describes a second-order phase transition, however, and it has a substantial mode softening, as mentioned above. These features differ from many ex-

perimental findings<sup>1,2</sup> which show that very few diffusionless structural transitions are second order, and most have only minor frequency softening for the modes which produce the displacive lattice correspondence. The consequence is that different considerations are necessary, which brings us to the research reported here; models which can deal with first-order transitions must be constructed.

Paralleling the development of the soft-mode models, a “Landau mean-field” description is constructed. A Landau free-energy function of the form<sup>12</sup> (see Fig. 1)

$$\frac{F}{F_0} = A(T) \frac{\eta^2}{2} - \frac{\eta^3}{3} + \frac{\eta^4}{4} + \dots, \quad (1.4)$$

describes a first-order transition; as before,  $\eta$  is the order parameter,  $A(T)$  a temperature-dependent control parameter, and  $F_0$  a scale energy. It is important to note that this function is asymmetric in  $\eta$  (the point symmetry of the high-temperature phase may dictate other forms for  $F$ ). The absolute minimum of  $F$  determines the equilibrium state; thus, for  $A(T) > \frac{2}{9}$ , the order parameter is  $\eta=0$ , for  $A(T) = \frac{2}{9}$ , the values  $\eta=0$  and  $\frac{2}{3}$  are degenerate, and for  $A(T) < 2/9$ ,  $\eta = \{1 + [1 - 4A(T)]^{1/2}\} / 2 > \frac{2}{3}$ . The order parameter jumps discontinuously as  $A(T)$  passes through  $\frac{2}{9}$ , which is the condition for the transition. Physically,  $\eta=0$  could correspond to a  $\beta$ -cubic phase, and  $\eta = \frac{2}{3}$  to a close-packed structure along  $[111]_{\text{cubic}}$ , for example.

Again, paralleling the soft-mode theory and the anharmonic phonon theories,<sup>6,7</sup> the coefficient  $A(T)$  can be related<sup>13</sup> to the quasiharmonic frequency of the mode generating the lattice correspondence, i.e.,  $A(T) \propto \omega_\eta^2$ . According to this mean-field theory, however,  $\omega_\eta^2$  approaches a *nonzero* value ( $\frac{2}{9}$  in the appropriate units) at

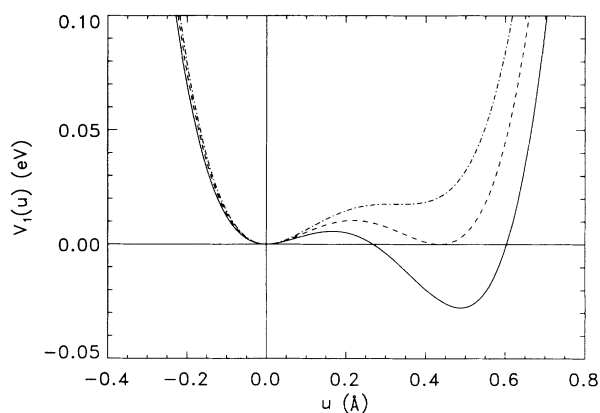


FIG. 1. This figure has two interpretations. The first is a plot of the Landau free-energy function  $F$  as a function of order parameter  $\eta$  of Eq. (1.4). The dot-dashed curve is for  $A(T) = \frac{1}{4}$ , the dashed curve is for  $A(T) = \frac{2}{9}$ , and the solid curve is for  $A(T)$  in the range  $0 < A(T) < \frac{2}{9}$ . The second interpretation is a plot of the on-site potential-energy function of Eq. (2.2); the solid curve is for the value  $a_0 = 1.50 \text{ eV}/\text{Å}^2$  used for the simulations (see Tables I and II).

the transition. In fact, little change in frequency occurs as  $A(T)$  moves through the transition.<sup>13</sup> Over some temperature range,  $A(T)$  can be represented by  $a(T - T_0)$ , just as in the soft-mode theory Eq. (1.1), but, as noted in Ref. 13,  $T_0$  may even be negative. Thus, this putative soft-mode instability temperature has little to do with the transition temperature, although the mode pattern still associates with the transformation lattice correspondence.<sup>14</sup> These observations can be fit by the heuristic models of Cook<sup>15</sup> and Krumhansl and Gooding.<sup>13</sup> However, again the questions of transformation precursors and detailed dynamics are not answered by the Landau mean-field approach.

To obtain information on these questions we continued to follow the strategy applied to the  $\phi^4$  model and turned to the computer simulation (as in Ref. 11) of models appropriate to first-order transitions. The comparison of the free energy Eq. (1.1) and potential energy Eq. (1.3) for the second-order transition of the  $\phi^4$  model suggested that, for a first-order transition, we should use a potential energy with the form of Eq. (1.4) but with *temperature-independent* parameters [see Eq. (2.2) below].<sup>16,17</sup> By using a *potential energy* with the same form as a Landau *free energy* which has a first-order transition, we expected to get the same form as *the* Landau free energy with appropriately temperature-dependent parameters.

However, the results obtained here, and also by Morris and Gooding,<sup>18</sup> show that expectation to have been somewhat simplistic, for good physical reasons. The physical argument goes back to Zener<sup>19</sup> (in 1947): If, at  $T=0$ , a low-symmetry structure [e.g., the  $\omega$  phase, or some (111) close-packed modification] has lower potential energy than a high-temperature structure (e.g.,  $\beta$  cubic), then the likely way by which the high-energy phase can have lower *free energy* at finite temperature is by having greater vibrational entropy, which is achieved by having lower-frequency phonons. In particular, the  $\beta$ -cubic structure has intrinsically very low-frequency  $\frac{2}{3}(1,1,1)$  or  $(1,1,0)$  phonons compared to those of the close-packed lower-temperature structure, which corroborates Zener's suggestion that the transition between the low- $T$  and high- $T$  structures is entropy driven. (See also the discussions of Ye *et al.* and of Willaime and Massobrio.<sup>20</sup>)

Having recognized the importance of the vibrational entropy in this context, we then had the problem of appropriately controlling the phonon frequencies in the simulation models while maintaining the desired form of the on-site potential energy (cf. the discussion in previous paragraph). We have done this by introducing an additional term in the *intersite* potential energy which stiffens the coupling in the  $\eta \neq 0$  (viz, close-packed or product) structure relative to the  $\eta = 0$  (viz,  $\beta$ -cubic or parent) structure. This term appears as an "anharmonic" coupling term between displacements at nearest-neighbor sites [cf. Eq. (2.4) below]. The importance of including this feature to incorporate physical realism into the model has become apparent from the simulations.

For clarity there are two additional points which merit attention here. First, in the discussion above, and also frequently in the literature, the variables  $\{u_i\}$  might appear to denote the actual atomic displacements. That

may be the case in some situations; however, if the mode(s) describing the lattice correspondence of the two phases is (are) at wave vector(s)  $\mathbf{q}_0$ , which are nonzero, then the  $u_i$  are really the modulation *amplitude*  $u_{q_0}(\mathbf{r}_i)$  of these significant modes; the actual displacement at site  $\mathbf{r}_i$  is  $u_{q_0}(\mathbf{r}_i)\cos(\mathbf{q}_0 \cdot \mathbf{r}_i)$ . Averaging over the rapidly varying  $\cos(\mathbf{q}_0 \cdot \mathbf{r}_i)$  terms produces an effective Hamiltonian in terms of these amplitudes  $u_{q_0}(\mathbf{r}_i)$ . The procedure for obtaining such effective Hamiltonians is discussed for a number of cases by Bruce, Cowley, and Murray.<sup>21</sup> Thus, one is to think of  $u_i$  as the amplitude (complex, in general) of the phonon  $\exp(i\mathbf{q}_0 \cdot \mathbf{r}_i)$  at position  $\mathbf{r}_i$ . For example, for the  $\omega$  phase, the significant phonon is the LA mode at  $\mathbf{q}_0 = \frac{2}{3}(1,1,1)$  and for the hcp " $\alpha$  phase" it is the  $TA_2$  mode at the  $N$  point (110) of the Brillouin zone.

Lastly, we mention two other interactions that may be important to this model, but which we are ignoring: order-parameter-strain coupling, and coupling between the distinct variants of the  $\omega$  phase that have different  $\mathbf{q}$  values. The strain that couples to the order parameter for this transition<sup>21</sup> is the symmetric strain. Thus, the part of the static physics that we are ignoring is that there is a small homogeneous volume change at the transition. While this is probably an irrelevant effect for the statics, the effect of the strain field on the dynamics is not necessarily small.<sup>22</sup> To be specific, we know that the long-ranged elastic force induced by any inclusions alters the classical nucleation rate, but for now we shall ignore this effect. The second interaction that we have ignored is that between domains of the product phase with different wave vectors belonging to the star of  $\mathbf{q} = \mathbf{q}_0$ . We do not expect this interaction to be important, as it is a high-order invariant that appears in the phenomenological free-energy expansion (fourth-order, in comparison to the third-order umklapp term that leads to the stability of the single-variant  $\omega$  phase<sup>13</sup>), and thus here we shall only consider one possible wave vector for the product phase. Thus, understanding that the simulation is effectively for the amplitude of a single-phonon eigenvector that does not include the coupling to homogeneous strains, we proceed to a detailed description of the model in Sec. II, of the molecular-dynamics techniques in Sec. III, and of the results in Sec. IV. Discussion and conclusions are in Sec. V.

## II. THE MODEL

As explained in the Introduction, the microscopic model used in this paper is a generalization of one that has been used extensively to study second-order structural phase transitions.<sup>4</sup> The first element of the model is a two-dimensional square lattice with  $N_x$  and  $N_y$  sites along the  $x$  and  $y$  axes, respectively; the total number of sites is  $N = N_x N_y$ . These sites are labeled by vectors  $\mathbf{n} = (n_x, n_y)$  whose components are integers restricted to lie in the ranges  $1 \leq n_x \leq N_x$ ,  $1 \leq n_y \leq N_y$ . The value of the displacement field at lattice site  $\mathbf{n}$  is denoted by  $u(\mathbf{n}) \equiv u(n_x, n_y)$ . This is a one-component or scalar field; that is, the model assumes that the significant displacements occur in only one direction. As discussed in the

Introduction, this field is actually the amplitude of the phonon mode which drives the displacive correspondence. Periodic boundary conditions are used, so that

$$u(n_x + N_x, n_y) = u(n_x, n_y + N_y) = u(n_x, n_y) .$$

The total potential-energy function  $\Phi$  is a sum of single-particle (on-site) terms and nearest-neighbor pair-interaction terms:

$$\Phi = \sum_{\mathbf{n}} V_1(u(\mathbf{n})) + \frac{1}{2} \sum_{\mathbf{n}, \delta} V_2(u(\mathbf{n}), u(\mathbf{n} + \delta)) . \quad (2.1)$$

Here  $\delta$  denotes the set of nearest-neighbor vectors in two dimensions  $[(\pm 1, 0)$  and  $(0, \pm 1)]$ .

The on-site potential is taken to be

$$V_1(u) = \frac{1}{2} a_0 u^2 - \frac{1}{3} B u^3 + \frac{1}{4} C u^4 , \quad (2.2)$$

where the parameters  $a_0$ ,  $B$ , and  $C$  are positive. We are interested in effects arising from changes in the *shape* of  $V_1(u)$ . From the three parameters, the overall scales of energy and displacement are determined by the combinations  $B^4/C^3$  and  $B/C$ , respectively. The shape is determined by the dimensionless ratio  $a_0/(B^2/C)$ . When this ratio is in the range  $0 < a_0/(B^2/C) < \frac{2}{9}$ ,  $V_1(u)$  is an asymmetric double well (Fig. 1) with the higher (metastable) minimum located at  $u_{ms}$  and the lower (stable) minimum located at  $u_s$ , where

$$u_{ms} = 0, \quad u_s = \left[ \frac{1 + \sqrt{1 - 4[a_0/(B^2/C)]}}{2} \right] \frac{B}{C} . \quad (2.3)$$

For  $a_0/(B^2/C) = \frac{2}{9}$ ,  $V_1(u)$  is a symmetric double well; this is the on-site potential usually considered in theories of second-order structural phase transitions.<sup>4</sup> (Usually the origin is taken at the maximum of the potential rather than at the left-hand minimum as we are doing here.) The single-particle potential is nontranslationally invariant for both symmetric and asymmetric cases. It is to be imagined to arise from an underlying sublattice whose atoms do not participate in the structural transition.<sup>4</sup>

For the pair-interaction term, we have used the anharmonic function

$$V_2(u(\mathbf{n}), u(\mathbf{n}')) = \frac{1}{2} \{ k + \alpha [u(\mathbf{n}) + u(\mathbf{n}')] \} \times [u(\mathbf{n}) - u(\mathbf{n}')]^2 \quad (2.4)$$

with harmonic force constant  $k$  and anharmonic force constant  $\alpha$ . [The anharmonic part is different from that in Ref. 18 because the on-site potential in Eq. (2.2) is asymmetric.] The motivation for this choice is the following. In the models for second-order transitions the interaction term is taken to be the nearest-neighbor *harmonic* interaction obtained by setting  $\alpha = 0$  in Eq. (2.4),

$$V_2(u(\mathbf{n}), u(\mathbf{n}'))|_{\alpha=0} = \frac{1}{2} k [u(\mathbf{n}) - u(\mathbf{n}')]^2 . \quad (2.5)$$

When this pair-interaction energy is combined with the *symmetric* on-site potential (cf. the previous paragraph), the resulting system is the so-called  $\phi^4$  model, which has been extensively studied.<sup>9-11</sup> For dimensionality  $d \geq 2$ , this system has a second-order phase transition. We found by computer simulation that *no* phase transition

occurs when the *harmonic* interaction [Eq. (2.5)] is combined with the *asymmetric* on-site potential in Eq. (2.2) for dimensionality  $d = 2$ . A way to understand this result is to note that the shape of the asymmetric on-site potential as a function of  $u$  is very similar to the shape of the symmetric potential plus a contribution from an external force acting on each particle, which adds a term  $-Fu$  in the potential energy for each particle. Whether the symmetry is removed by a cubic term or by a linear term does not seem to be important. It is known that an external field destroys a second-order transition that is present without the field. The results of our earlier simulations are consistent with the fact.

In order to produce a first-order transition (for  $d \geq 2$ ), we introduce the additional anharmonic term proportional to the parameter  $\alpha$  in Eq. (2.4). From the form of that function one sees that this term effectively makes the force "constant" of the spring (bond) joining a nearest-neighbor pair of particles dependent on the position of the center of mass of the pair. We take  $\alpha > 0$  so that the force "constant" is larger when both particles are near the stable minimum of the on-site potential  $V_1(u)$  than when both are near the metastable minimum or when there is one particle near each minimum. For temperatures near the transition, we imagine that the system organizes itself into clusters within which the particles are nearly all in one phase: either the metastable phase with the average displacement  $\langle u \rangle$  near  $u_{ms} = 0$  or the stable phase with  $\langle u \rangle$  near  $u_s$  [Eq. (2.3)]. The position dependence of the force "constant" causes the local (within a cluster) lattice vibrational frequencies to be higher in the clusters of the stable phase than in the clusters of the metastable phase. Because of the inverse relation between vibration frequencies and entropy,<sup>23</sup> this change increases the entropy of configurations which have more or larger clusters of the metastable phase. Through this mechanism, the anharmonic pair potential in Eq. (2.4) causes an entropy-driven phase transition<sup>18</sup> between these two configurations for dimensions  $d \geq 2$ .

The added terms in the pair-interaction potential are not translationally invariant. In this respect they are like the on-site potential  $V_1(u)$  and can be thought of in the same way as arising from the background sublattice of atoms that do not take part in the transition but do affect the potential energy between the atoms that are involved.<sup>4</sup>

The equations of motion obtained from the potential energy in Eqs. (2.1), (2.2), and (2.4) are

$$M\ddot{u}(\mathbf{n}) = -a_0 u(\mathbf{n}) + B u^2(\mathbf{n}) - C u^3(\mathbf{n}) + \sum_{\delta} [u(\mathbf{n} + \delta) - u(\mathbf{n})] \times \{ k + \frac{1}{2} \alpha [u(\mathbf{n} + \delta) + 3u(\mathbf{n})] \} . \quad (2.6)$$

These equations can be linearized for small oscillations about either the stable or metastable minimum of the on-site potential. The resulting linear equations are

$$M\ddot{u}(\mathbf{n}) = -(a_0 - 2B u_0 + 3C u_0^2) u(\mathbf{n}) + \sum_{\delta} (k + 2\alpha u_0) [u(\mathbf{n} + \delta) - u(\mathbf{n})] , \quad (2.7)$$

where  $u_0$  denotes either  $u_{\text{ms}}=0$  or  $u_s$  [Eq. (2.3)], depending on which point is chosen for the linearization. (In the continuum limit, this is a 2D Klein-Gordon equation.) The solutions of these equations are propagating lattice waves. The dispersion relations are ( $l$  is the lattice constant,  $\mathbf{q}$  the wave vector)

$$M[\omega^{(s)}(\mathbf{q})]^2 = a_0 - 2Bu_s + 3Cu_s^2 + 4(k + 2\alpha u_s) \times \left[ \sin^2 \left[ \frac{q_x l}{2} \right] + \sin^2 \left[ \frac{q_y l}{2} \right] \right], \quad (2.8)$$

for small oscillations about the stable minimum, and

$$M[\omega^{(\text{ms})}(\mathbf{q})]^2 = a_0 + 4k \left[ \sin^2 \left[ \frac{q_x l}{2} \right] + \sin^2 \left[ \frac{q_y l}{2} \right] \right], \quad (2.9)$$

for small oscillations about the metastable minimum. For the parameter values we have used in the simulations (cf. next section), the curvature of the on-site potential is greater at the stable minimum than at the metastable minimum [i.e.  $(a_0 - 2Bu_s + 3Cu_s^2) > a_0$ ], and so near  $\mathbf{q}=0$ , where  $\alpha$  has no effect, Eqs. (2.8) and (2.9) show that the phonons in the stable well have higher frequency than those in the metastable well. Furthermore, comparison of the coefficients of the  $\mathbf{q}$ -dependent term shows that the anharmonicity introduced through the parameter  $\alpha$  increases the bandwidth of the phonon spectrum for small oscillations about the stable minimum. This observation is relevant for the results presented in Sec. IV.

Inspection of Eqs. (2.1), (2.2), and (2.4) suggests that the minimum-energy configuration (which is the  $T=0$  structure) of the system is spatially uniform. Equation (2.4) is then zero, and the value of the uniform displacement minimizes the on-site potential, which is  $u_s$  in Eq. (2.3). However, because the anharmonic term proportional to  $\alpha$  is *cubic*, it can take on large negative values; this possibility allows spatially nonuniform structures to have lower energies for sufficiently large  $\alpha$  values. We now explain this *caveat*.

We consider the 2D square lattice to be composed of two interpenetrating sublattices  $A$  and  $B$  with the property that the nearest neighbors of every  $A$  site are  $B$  sites and *vice versa*. If the displacements within each sublattice are uniform with the values  $U_A$  and  $U_B$ , then the potential energy of this configuration is

$$\Phi = \frac{N}{2} V_1(U_A) + \frac{N}{2} V_1(U_B) + N[k + \alpha(U_A + U_B)](U_A - U_B)^2. \quad (2.10)$$

In terms of the center-of-mass (c.m.) displacement  $U_{\text{c.m.}} = (U_A + U_B)/2$  and the relative displacement  $u_r = U_A - U_B$ , this energy is

$$\Phi = \frac{N}{2} V_1(U_{\text{c.m.}} + \frac{1}{2}u_r) + \frac{N}{2} V_1(U_{\text{c.m.}} - \frac{1}{2}u_r) + N(k + 2\alpha U_{\text{c.m.}})u_r^2. \quad (2.11)$$

The location of the extrema of this expression are found by setting the derivatives with respect to  $U_{\text{c.m.}}$  and  $u_r$  to zero. When we introduce the explicit form of  $V_1$  from Eq. (2.2) and use the fact that we are seeking nonuniform solutions so that  $u_r \neq 0$ , we obtain

$$2a_0 U_{\text{c.m.}} - B(2U_{\text{c.m.}}^2 + \frac{1}{2}u_r^2) + C(2U_{\text{c.m.}}^3 + \frac{3}{2}U_{\text{c.m.}}u_r^2) + 4\alpha u_r^2 = 0 \quad (2.12)$$

and

$$(a_0 + 8k) + (16\alpha - 2B)U_{\text{c.m.}} + 3CU_{\text{c.m.}}^2 + \frac{1}{4}Cu_r^2 = 0. \quad (2.13)$$

The c.m. and relative variables can now be separated by solving Eq. (2.13) for  $u_r^2$ ,

$$u_r^2 = - \left[ 12U_{\text{c.m.}}^2 + 8 \left[ \frac{8\alpha - B}{C} \right] U_{\text{c.m.}} + 4 \left[ \frac{a_0 + 8k}{C} \right] \right], \quad (2.14)$$

and substituting in Eq. (2.12) to give

$$CU_{\text{c.m.}}^3 + (9\alpha - B)U_{\text{c.m.}}^2 + \frac{1}{4} \left[ a_0 + 12k + \frac{(8\alpha - B)^2}{C} \right] U_{\text{c.m.}} + \frac{1}{8C} (a_0 + 8k)(8\alpha - B) = 0. \quad (2.15)$$

From this point we proceed numerically, taking  $a_0$ ,  $B$ ,  $C$ ,  $k$  fixed at the values used for the simulation and considering a range of  $\alpha$  values. The roots of Eq. (2.15) are found, giving the possible  $U_{\text{c.m.}}$  values. These values substituted into Eq. (2.14) give the possible  $u_r$  values. The energies of these solutions are obtained from Eq. (2.11). The results are shown in Fig. 2. For  $\alpha \leq 5.96 \text{ eV/\AA}^3$ , there are no real solutions of Eqs. (2.14) and (2.15), whereas for  $\alpha$  larger than this value there are two real

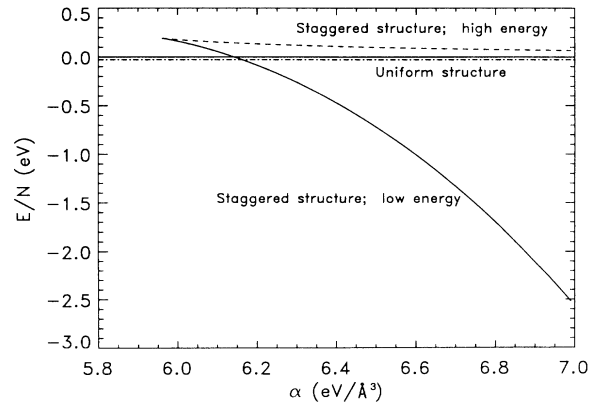


FIG. 2. Energy per particle vs anharmonicity parameter  $\alpha$  for the two-sublattice structure discussed in the text. The curves labeled “staggered structure” are the energies of the two real solutions of Eqs. (2.14) and (2.15), calculated from Eq. (2.11). The constant value labeled “uniform structure” is the minimum of the on-site potential  $V_1(u)$ .

solutions. The energy of one of these decreases rather rapidly with increasing  $\alpha$  and for  $\alpha \geq 6.16 \text{ eV/\AA}^3$  it lies below the energy of the uniform solution. Thus, this nonuniform solution is the stable structure at  $T=0$  for these larger  $\alpha$  values.

The simulations described in the following sections are all for  $\alpha$  values less than this critical value, so that the  $T=0$  structure is spatially uniform at the stable minimum of  $V_1(u)$ . However, it is useful to keep in mind that the model contains possibilities for more complicated structures.<sup>24</sup>

### III. MOLECULAR-DYNAMICS CALCULATIONS

The equations of motion used for the simulations are given in Eq. (2.6). These equations are integrated by an algorithm due to Beeman,<sup>25</sup> which is deterministic and conservative (microcanonical ensemble). Additional damping and stochastic terms, to represent the interaction of the system with a heat bath (canonical ensemble), are not included.

The values for the mass  $M$ , and the potential-energy parameters  $a_0$ ,  $B$ ,  $C$ , and  $k$  are given in Table I. They are chosen to represent zirconium, which has a much-studied structural transition from a high-temperature  $\beta$ -cubic phase to a low-temperature  $\omega$  phase. The values for  $a_0$ ,  $B$ , and  $C$  are obtained by fitting the cubic polynomial  $V_1(u)$  in Eq. (2.2) to frozen phonon calculations of the energy as a function of the amplitude for the  $\frac{2}{3}(1,1,1)$  phonon of Zr, done by Ho *et al.*<sup>26</sup> (Those calculations are not accurately fit by a cubic polynomial, so the simulations cannot be expected to be an accurate description of real Zr.) The value for  $k$  was obtained to fit<sup>27</sup> the curvature in the longitudinal direction at the minimum at  $\frac{2}{3}(1,1,1)$  of the observed phonon dispersion curves for Zr.<sup>28</sup> (The phonon dispersion of Zr is highly anisotropic about this point so that a force-constant tensor is required to describe it accurately rather than a single  $k$ . This is another reason these simulations cannot be an accurate description of Zr.)

A value for the parameter  $\alpha$  for Zr is not available, so we used theoretical considerations to determine a reasonable range of values. Equation(2.8) shows that the change of phonon frequencies for the low-temperature phase from Brillouin-zone center to boundary is governed by the combinations  $(k + 2\alpha u_s)$ . The decrease of the phonon frequencies from the low-temperature structure to the high-temperature structure is the mechanism for producing the entropy-driven transition between the phases. Thus, it seemed reasonable to consider  $\alpha$  values

in the range from zero to where  $\alpha u_s \approx k$ . Thus, given the values of the other parameters, we have done simulations for several values in the range  $0 \leq \alpha \leq 3.40 \text{ eV/\AA}^3$ .

Certain energy comparisons determined by these numbers are of interest. The maximum and minimum of  $V_1(u)$  (Fig. 1) are  $V_{\max} = 5.73 \text{ meV}$  and  $V_{\min} = -27.9 \text{ meV}$ . For the interparticle interaction energy, first consider the case where  $\alpha=0$ . The interaction energy required to move one particle from the metastable minimum to the maximum of the on-site potential, all other atoms remaining fixed, is (recall that this displacement stretches four springs)  $2ku_{\max}^2 = 96.2 \text{ meV}$ . Similarly, the interaction energy to move a particle from the stable minimum to the maximum is  $2k(u_{\min} - u_{\max})^2 = 346 \text{ meV}$ . If we now include the effect of  $\alpha$ , these numbers become even larger. Thus, for displacement of a particle out of either well, the interaction (bond) energy is larger than the corresponding site energy. A system with this ordering of the energies is said to be displacive;<sup>4</sup> the larger bond energy tends to cause the particle displacements to vary slowly as a function of site position.

Integration of Eq. (2.6) is simplified by rewriting them in terms of dimensionless units. The factors for doing that conversion are given in Table II; the effect is to make  $M=B=C=1$  and, of course, to change the values of  $a_0$ ,  $k$ , and  $\alpha$ .

The equations are integrated for a system of 6000 particles, with  $N_x=80$ ,  $N_y=75$ . The time step for the integration is chosen to be  $\Delta t = 2.74 \times 10^{-15} \text{ sec}$ . With this time step the energy is conserved to within a few parts in  $10^6$ . For one of our  $\alpha$  values ( $3.40 \text{ eV/\AA}^3$ ), two different series of runs were carried out: a "cooling" series, started at high temperature and a "heating" series started at low temperature. For other  $\alpha$  values only a "heating" series of runs was performed. The initial conditions for the beginning step of each of these series were random positions and velocities approximately appropriate for the starting temperatures. The initial conditions for the other temperature values in both series were derived from the position and velocity data at the end of the previous temperature step by cooling or heating the system.

The procedure for changing the temperature is as follows. The actual temperature is estimated from a short run of 1400 time steps. If it is not equal to the desired temperature to within a certain tolerance, then over the next 1400 time steps, the velocities are gently adjusted to

TABLE I. Values of parameters.

Quantity	Value
$M$	$1.49 \times 10^{-22} \text{ g}$
$a_0$	$1.50 \text{ eV/\AA}^2$
$B$	$12.1 \text{ eV/\AA}^3$
$C$	$18.5 \text{ eV/\AA}^4$
$k$	$1.67 \text{ eV/\AA}^2$

TABLE II. Units.

Unit	Formula	Value
Length	$B/C$	$0.654 \text{ \AA}$
Energy	$B^4/C^3$	$3.39 \text{ eV}$
Mass	$M$	$1.49 \times 10^{22} \text{ g}$
Time	$(MC)^{1/2}/B$	$3.43 \times 10^{-14} \text{ sec}$
Frequency	$B/(MC)^{1/2}$	$2.92 \times 10^{13} \text{ sec}^{-1}$
Force	$B^3/C^2$	$5.18 \text{ eV/\AA}$
Harmonic force constant	$B^2/C$	$7.91 \text{ eV/\AA}^2$
Cubic force constant	$B$	$12.1 \text{ eV/\AA}^3$
Quartic force constant	$C$	$18.5 \text{ eV/\AA}^4$

move the temperature toward the desired value. Next the system evolves undisturbed for 5600 time steps, and then a new actual temperature is calculated over the next 1400 steps. This process is repeated until the desired temperature is achieved. Then the system is “aged” for 50 000–100 000 time steps, while monitoring the temperature, specific heat, and the fourth and sixth moments of the velocity distribution. After thermal equilibrium is obtained, the equations are integrated for  $10^{-9}$  sec of real time, which is approximately 360 000 time steps. The data necessary for the computation of phase-space trajectory averages are accumulated on every tenth integration step.

The various thermodynamic averages are computed from the following formulas. The temperature is obtained from the average kinetic energy,

$$\frac{1}{2}Nk_B T = \left\langle \sum_{\mathbf{n}} \frac{1}{2}M [v(\mathbf{n})]^2 \right\rangle \quad (3.1)$$

where  $v(\mathbf{n})$  is the velocity of the  $n$ th particle, and  $\langle \dots \rangle$  denotes a time average. The specific heat is obtained from the two formulas<sup>29</sup>

$$C = \frac{1}{2 - 4\langle(\Delta K)^2\rangle/NT^2} = \frac{1}{2 - 4\langle(\Delta\Phi)^2\rangle/NT^2}, \quad (3.2)$$

where  $\langle(\Delta K)^2\rangle$  and  $\langle(\Delta\Phi)^2\rangle$  are the mean-square fluctuations in kinetic and potential energies, respectively. Since the total energy is conserved, these two quantities are, in principle, equal; when evaluated from the molecular-dynamics (MD) data, they are not equal due to numerical errors. In presenting results in the next section, the average of the two formulas is given.

The order parameter  $\eta$  for the system is the average displacement, averaged over all sites and over time,

$$\eta = \langle P \rangle = \left\langle \frac{1}{N} \sum_{\mathbf{n}} u(\mathbf{n}) \right\rangle. \quad (3.3)$$

At very high temperatures this approaches the metastable minimum  $u_{ms}=0$ , and at very low temperatures it approaches the stable minimum  $u_s$  [Eq. (2.3)]. The displacement susceptibility is obtained from the displacement fluctuations

$$\chi = \frac{N}{k_B T} (\langle P^2 \rangle - \langle P \rangle^2). \quad (3.4)$$

The correlation of displacement fluctuations on two sites separated by lattice vector  $\mathbf{n}$  is measured by

$$\begin{aligned} g(\mathbf{n}) &= \left\langle \frac{1}{N} \sum_{\mathbf{n}'} [u(\mathbf{n}+\mathbf{n}') - \langle P \rangle][u(\mathbf{n}') - \langle P \rangle] \right\rangle, \\ &= \left\langle \frac{1}{N} \sum_{\mathbf{u}'} u(\mathbf{n}+\mathbf{n}')u(\mathbf{n}') \right\rangle - \langle P \rangle^2. \end{aligned} \quad (3.5)$$

We obtain the probability distribution function for the displacements from the MD data. At every data-taking step, the displacements of all particles are sorted into a histogram. The average of these histograms over the entire run, suitably normalized, gives the distribution.

Spectral functions for time-dependent correlation functions are also obtainable from the MD data. We present

results for the wave-vector-dependent displacement correlations in the next section. This spectral function is the one-phonon approximation to the scattering law for inelastic neutron scattering. The solutions  $u(\mathbf{n}, t)$  of the equations of motion are Fourier transformed with respect to both space and time to obtain

$$u_{t_{\max}}(\mathbf{q}, \omega) = \int_{-t_{\max}}^{t_{\max}} dt \sum_{\mathbf{n}} \exp[-i(\mathbf{q} \cdot \mathbf{n}l - \omega t)] u(\mathbf{n}, t). \quad (3.6)$$

The spectral function is then, according to the Wiener-Khinchin theorem,<sup>30</sup>

$$D(\mathbf{q}, \omega) = \lim_{t_{\max} \rightarrow \infty} \frac{1}{2t_{\max}} \frac{1}{N} |u_{t_{\max}}(\mathbf{q}, \omega)|^2. \quad (3.7)$$

The actual spectrum calculation also includes smoothing the data and averaging spectra from several overlapping time series.

#### IV. RESULTS

Figure 3 shows the energy as a function of the temperature for both the “cooling” and “heating” series at  $\alpha = 3.4 \text{ eV/\AA}^3$ . The discontinuity in the “heating” series, with the “discontinuity temperature”  $T_1$  between  $T = 936.77$  and  $936.99$  K, is reminiscent of the behavior of a system undergoing a first-order phase transition. No discontinuity occurred in the “cooling” series down to 200 K, even though we tried different tactics to cause one (for example, lowering the temperature through a large amount, say from 2000 to 600 K, rather than from just the next higher temperature in the series). Since hysteresis evidently occurs here, the temperature at this discontinuity is somewhere above the true transition temperature.

It is interesting to follow the “time dependence” of the temperature as it is raised through this transition, using the procedure described in Sec. III. Table III shows the series of “actual temperature” values as we raised the temperature in the “heating” series from just below the

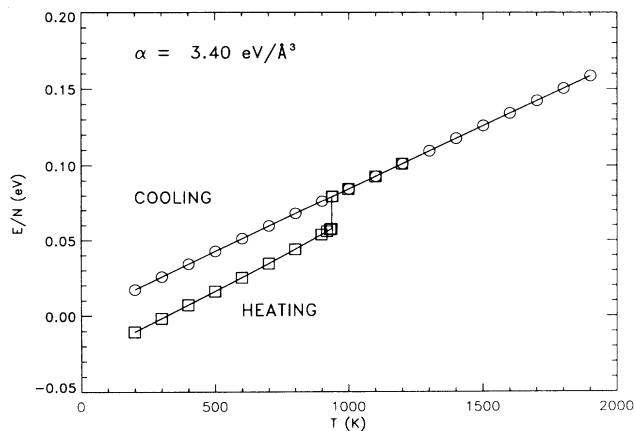


FIG. 3. Energy per particle vs temperature at  $\alpha = 3.40 \text{ eV/\AA}^3$  for both “heating” (squares) and “cooling” (circles).

TABLE III. History of temperature changes (in K) on heating through the transition. (Heating procedure is described in Sec. III.)

$\alpha=2.00 \text{ eV/\AA}^3$	$\alpha=3.40 \text{ eV/\AA}^3$
1070.1	936.4
1072.2	935.7
1067.0	935.2
1071.4	937.5
1073.3	936.6
1037.2	937.3
1039.3	680.8
1034.1	805.2
1004.6	871.3
946.6	904.5
1009.3	921.2
1041.4	929.2

transition to just above it, for two different  $\alpha$  values. (For  $\alpha=2.00 \text{ eV/\AA}^3$ , we are going from 1068 to 1070 K, and for  $\alpha=3.40 \text{ eV/\AA}^3$  from 936.77 to 937 K.) Partway through these small increases, the temperature falls dramatically, showing that many particles move into the metastable well of the on-site potential at  $u_{ms}=0$  (Fig. 1). (The spatial distribution of the particles is presented more precisely later in this section.) Since the energy is conserved, except at the instants when the velocities are adjusted to move the temperature toward the desired

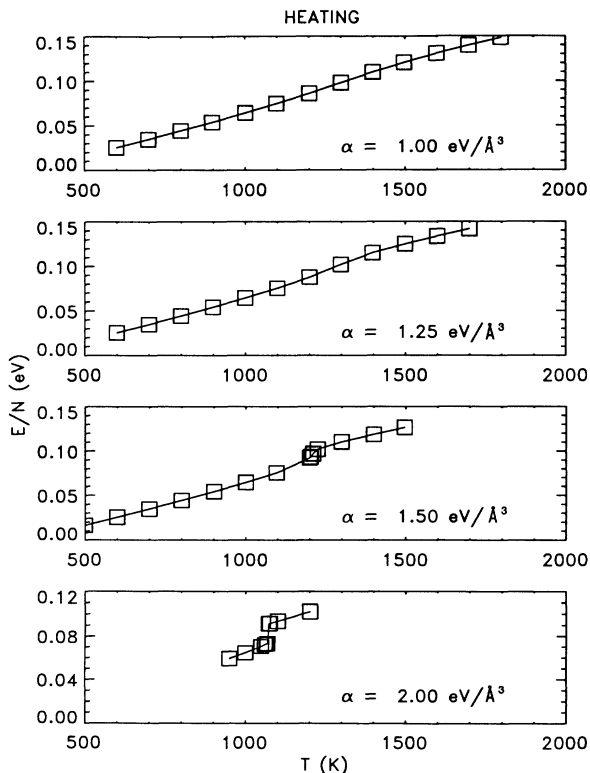


FIG. 4. Energy per particle vs temperature for several  $\alpha$  values. All are obtained for “heating.”

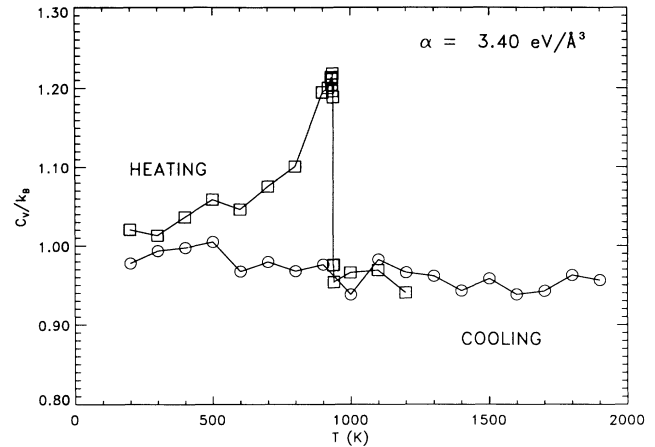


FIG. 5. Specific heat (per particle) in units of Boltzmann's constant vs temperature for  $\alpha=3.40 \text{ eV/\AA}^3$ . Squares show “heating” values, circles show “cooling” values.

value, the kinetic energy and the temperature fall when the particles shift their positions. After this sudden change in the spatial configuration, the “heating” procedure continues to move the temperature toward the desired value (which took several adjustments beyond those shown in Table III).

From seeing how the transition occurs in the “heating”

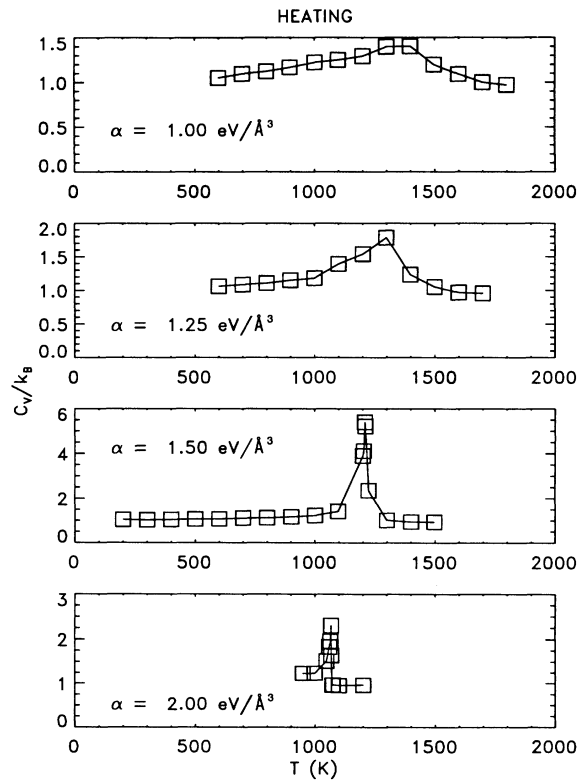


FIG. 6. Specific heat (per particle) vs temperature for several  $\alpha$  values. All are obtained for “heating.” Notice the changes in the vertical scales, especially for  $\alpha=1.50 \text{ eV/\AA}^3$ .

series, one can speculate that having a transition occur on cooling would be difficult. In a “cooling” transition the particles would be moving from the metastable to the stable well, thereby decreasing potential energy and increasing kinetic energy. But increasing the kinetic energy increases the temperature, which tends to return the particles to the metastable well where they started. Thus, the energy-conserving MD algorithm we have used may inhibit a transition on cooling. A Langevin or constant-temperature MD method, incorporating damping and noise forces which could absorb the energy released at a “cooling” transition, may be better suited to study this transition.

Figure 4 shows the energy per particle as a function of temperature for several smaller values of  $\alpha$ . For the two smaller values of  $\alpha$ , this function is smooth and shows there is no transition, whereas at  $\alpha = 1.50 \text{ eV/\AA}^3$  there is evidence for a transition. The major conclusion from this series of graphs is that a minimum strength of interparticle anharmonicity is required to produce a transition. The evidence from this  $E$  vs  $T$  graph and from other thermodynamic functions presented below is that the critical value of  $\alpha$  to produce a transition is close to  $\alpha = 1.50 \text{ eV/\AA}^3$  (this value is, of course, a function of the other parameters in the model). It is possible that, at the critical  $\alpha$ , the transition is continuous, i.e., second order. This possibility will be discussed further after the other thermodynamic functions are discussed. A further result from Figs. 3 and 4 is that  $T_1$ , the “discontinuity temperature,” decreases with increasing  $\alpha$ . This decrease occurs because increasing  $\alpha$  produces a larger entropy difference between the two structures, thereby stabilizing the high-temperature phase to a lower temperature.

The specific heat is shown in Fig. 5 at  $\alpha = 3.40 \text{ eV/\AA}^3$  for both the “heating” and “cooling” series and in Fig. 6 for the smaller values of  $\alpha$ . In Fig. 5,  $C_v$  appears to signal the transition when it is approached from below but not on approach from above. In Fig. 6 for  $\alpha = 1.50 \text{ eV/\AA}^3$ , the curve could be interpreted as a  $\lambda$ -type singularity seen at second-order transitions (note the vertical

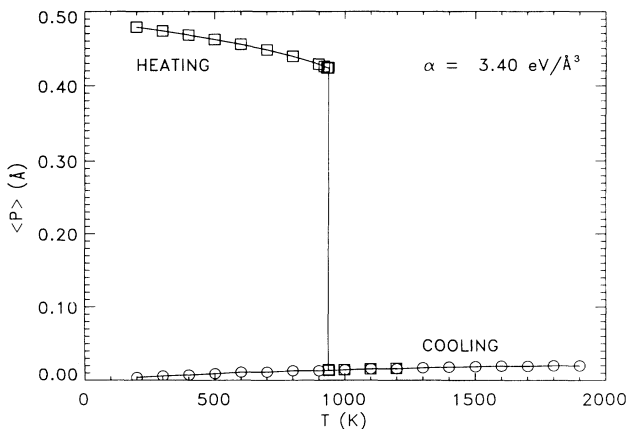


FIG. 7. Order parameter vs temperature at  $\alpha = 3.40 \text{ eV/\AA}^3$  for both “heating” (squares) and “cooling” (circles).

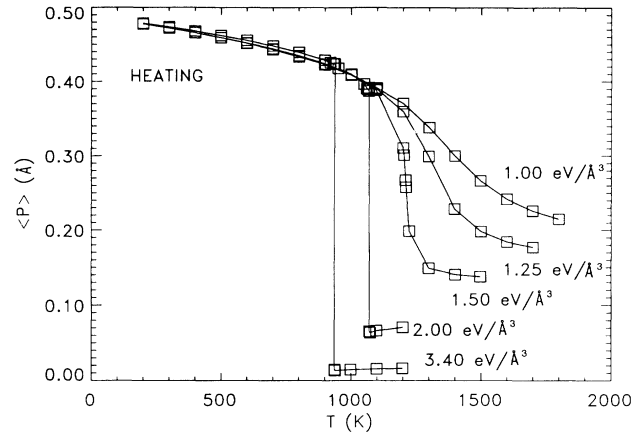


FIG. 8. Order parameter vs temperature for several  $\alpha$  values. All are obtained for “heating.”

scale change). This is part of the evidence that this value of  $\alpha$  is close to “critical.”

The next two figures are related directly to the structural change which occurs at the transition. Figure 7 shows the order parameter [Eq. (3.3)] for both heating and cooling at  $\alpha = 3.40 \text{ eV/\AA}^3$  and Fig. 8 shows it for heating at smaller  $\alpha$  values. This quantity is discontinuous for the larger  $\alpha$  values and smooth for the smaller values. The hysteresis for the case where we have “heating” and “cooling” runs is clearly evident. At  $\alpha = 1.50 \text{ eV/\AA}^3$  this function could be interpreted to be continuous but with diverging slope, again showing the closeness to a critical  $\alpha$ .

The order-parameter susceptibility is in Fig. 9 at  $\alpha = 3.40 \text{ eV/\AA}^3$  for both “heating” and “cooling.” The heating curve shows similar behavior to the specific heat in that it appears to signal the transition. Figure 10 shows the susceptibility for the smaller  $\alpha$  values and again presents evidence that  $\alpha = 1.50 \text{ eV/\AA}^3$  is close to “critical.”

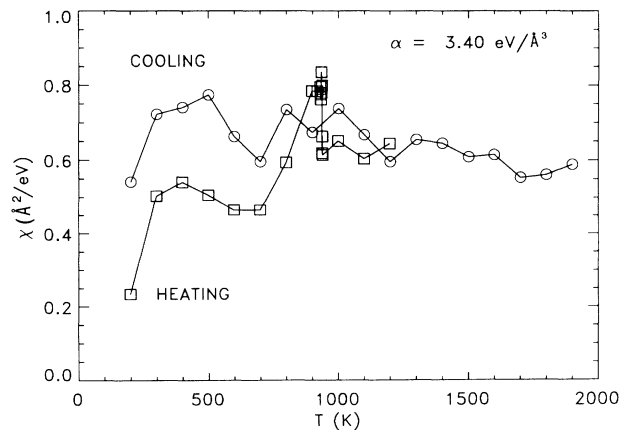


FIG. 9. Displacement susceptibility vs temperature at  $\alpha = 3.40 \text{ eV/\AA}^3$  for both “heating” (squares) and “cooling” (circles).

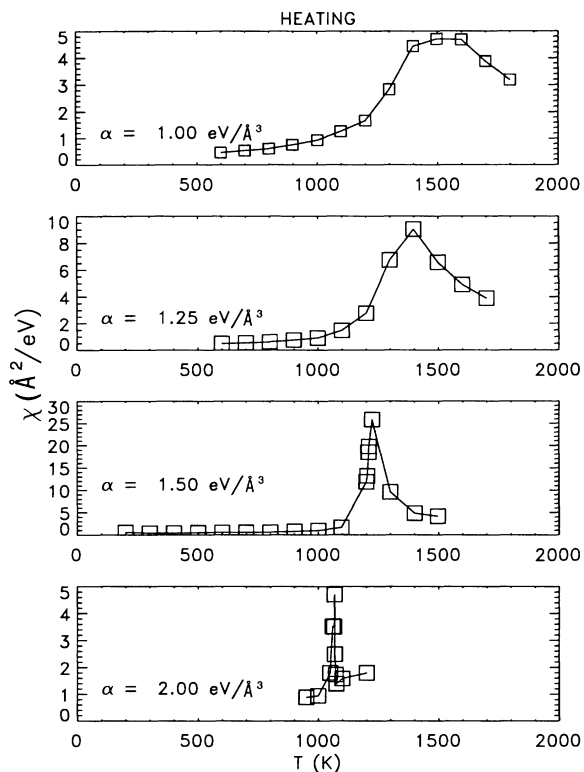


FIG. 10. Displacement susceptibility for several  $\alpha$  values. All are obtained for “heating.” Notice the changes in vertical scale, especially at  $\alpha = 1.50 \text{ eV/\AA}^3$ .

The preceding discussion has referred to the possibility that there is a critical value of  $\alpha$  (close to  $1.50 \text{ eV/\AA}^3$  for our parameter values) necessary for a first-order transition and that the temperature dependence of the thermodynamic functions suggests a second-order transition at the critical value. The situation appears analogous to the van der Waals fluid with the critical temperature being the analogue of the critical  $\alpha$ , in the sense that decreasing

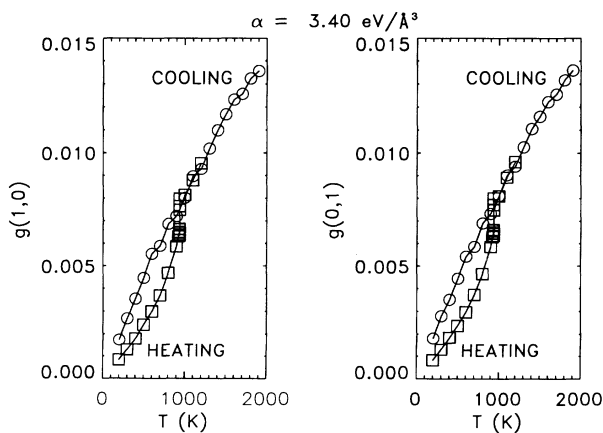


FIG. 11. Displacement correlation function [Eq. (3.5)] for  $\alpha = 3.40 \text{ eV/\AA}^3$  at separation of one lattice constant in both the  $x$  and  $y$  directions, as functions of temperature. Squares show “heating” values and circles show “cooling” values.

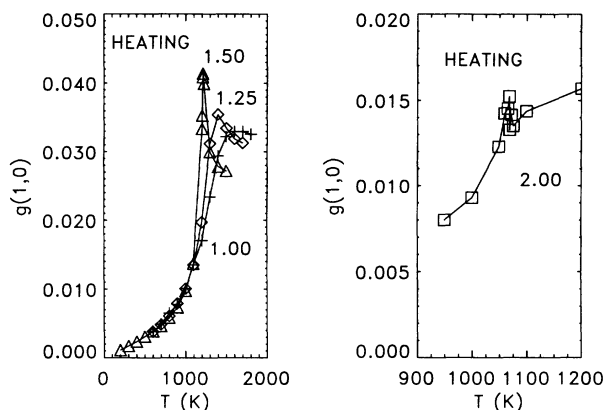


FIG. 12. Displacement correlation for several  $\alpha$  values at separation of one lattice constant in the  $x$  direction vs temperature. All are “heating” values. The left panel is for  $\alpha$  values up to the critical value, and the right is for values larger than critical. The  $\alpha$  values on the left panel are as follows: plus signs,  $1.00 \text{ eV/\AA}^3$ ; diamonds,  $1.25 \text{ eV/\AA}^3$ ; triangles,  $1.50 \text{ eV/\AA}^3$ .

$\alpha$  produces a line of first-order phase transitions which terminates at a second-order transition. However, one should recall that the simulations are for a small number of particles; it is possible that the second-order critical temperature would scale to zero for increasing particle number. Another possibility is that some variety of multicritical phenomenon occurs here. However, these possibilities are peripheral to our objective to study the dynamics of the first-order transition at the larger  $\alpha$  values.

The next three figures are related to the static displacement correlation function [Eq. (3.5)]. Figure 11 is for  $\alpha = 3.40 \text{ eV/\AA}^3$  and shows the correlation at one unit of separation along both the  $x$  and  $y$  axes as functions of temperature. The two functions are essentially equal, which shows the isotropy of the system. For this  $\alpha$  value these functions are monotonically increasing at all temperatures and appear to have a diverging slope at the transition (in the “heating” series). Figure 12 shows  $g(1,0)$  for the smaller  $\alpha$  values (and all for “heating”). For the  $\alpha$ 's below the “critical” value,  $g(1,0)$  goes through a maximum, with the  $\alpha = 1.50 \text{ eV/\AA}^3$  curve possibly showing a divergence. For  $\alpha = 2.00 \text{ eV/\AA}^3$  the case appears to be discontinuous at the transition as opposed to the  $\alpha = 3.40 \text{ eV/\AA}^3$  case which appears continuous but with a diverging slope. Finally, Fig. 13 shows the spatial dependence  $g(n_x, 0)$  for  $\alpha = 3.40 \text{ eV/\AA}^3$  just above the transition ( $T = 936.99 \text{ K}$ ) and far above it ( $T = 1800.3 \text{ K}$ ). Since the two graphs are nearly parallel on this semilogarithmic plot, there is essentially no increase in the range of correlation over this temperature interval. This result is very different from the behavior of the same function at the second-order transition of the 2D  $\phi^4$  system (see, e.g., Figs. 6 and 8 of Ref. 11), which, of course, is characterized by a diverging correlation length.

The next series of figures shows the position probability distributions for several  $\alpha$  values. Figure 14 shows  $\alpha = 3.40 \text{ eV/\AA}^3$  for both “cooling” and “heating.” The

“cooling” series just shows the distribution becoming narrower in the metastable well of the on-site potential. The “heating” series shows the jump in the center of the distribution from the stable to the metastable well. The most remarkable feature of these distributions is that each has only a single maximum even very close to the transition. That is, the distributions do *not* show any marked tendency for particles to cluster in configurations appropriate to the “other” phase either above or below the transition (heterophase fluctuations). The only indication of such a tendency is seen in the “heating” series for temperatures below the transition. The centers of the distributions are slightly to the left of the stable minimum of the on-site potential  $u_s$ , [Eq. (2.3)], and the distributions are slightly asymmetric, with a longer tail to the small- $u$  side, toward the metastable minimum. One way to quantify this tendency is to calculate the *kurtosis* of the distribution, which is the ratio of the fourth moment to the square of the second moment. For a Gaussian distribution the kurtosis has the value 3, and so larger (smaller) values of the kurtosis indicate more (less) weight in the wings compared with the Gaussian. Because the on-site potential is asymmetric about its minima, the distribution is never exactly Gaussian in any situation. However, the temperature dependence of the kurtosis shows the wings grow and then contract as  $T$  goes through the transition. Values of the kurtosis are in Table IV.

Figure 15 shows the probability distributions for the smaller  $\alpha$  values (“heating” series only). These distributions show the same asymmetry as the larger  $\alpha$  distribution (see the kurtosis values in Table IV). In all cases the kurtosis goes through a maximum at the transition and then falls to a value less than 3. (For  $\alpha=1.25$  eV/Å<sup>3</sup>, where there is no transition, the kurtosis maximum coincides with the specific-heat maximum.) However, we found no instance of a distribution with two maxima for these  $\alpha$  values.

The next set of figures is related to the dynamic displacement correlation function or spectral function  $D(\mathbf{q}_0, \omega)$  [E. (3.7)]. These are for the single value  $\alpha=3.40$  eV/Å<sup>3</sup> and are all from the “heating” series. Figure 16(a)

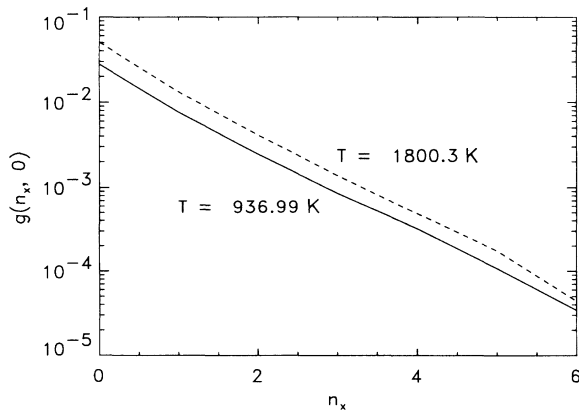


FIG. 13. Displacement correlation function [Eq. (3.5)] at  $\alpha=3.40$  eV/Å<sup>3</sup> as a function of lattice site separation for temperatures just above (solid line) and far above (dashed line) the transition.

is for a low temperature and Figs. 16(b) and 16(c) are for temperatures slightly below and above the transition. The components of the wave vector  $\mathbf{q}$  are noted on each plot, expressed as fractions of the zone boundary wave vector (i.e.,  $\mathbf{q}l/\pi$ ), and the frequencies are expressed as  $\omega/\omega_0$ , where  $\omega_0$  is the frequency unit given in Table II. Each spectral function is plotted on semilogarithmic axes to emphasize important low-intensity features; however, such a plot exaggerates the width of the phonon peaks,

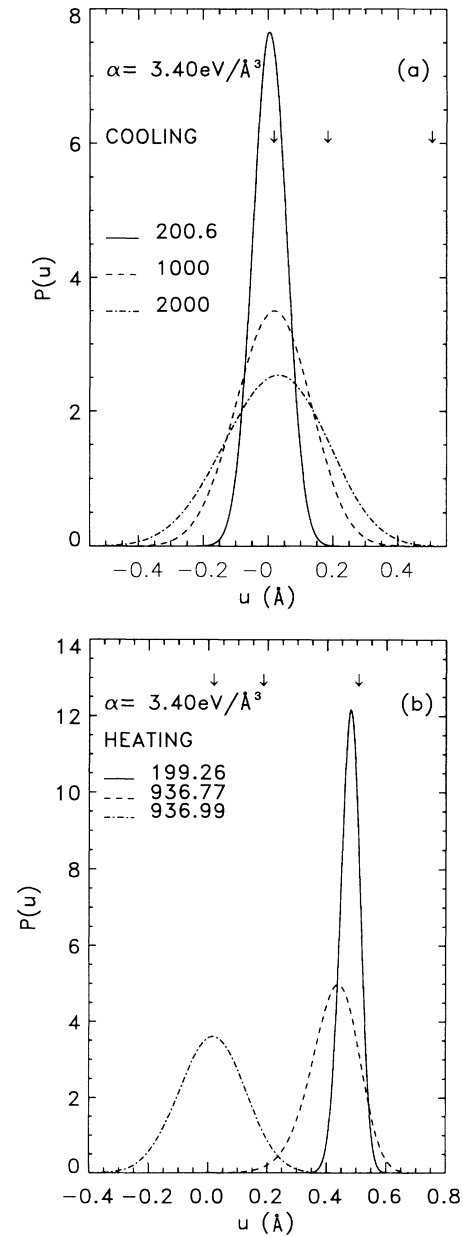


FIG. 14. Position probability distributions at  $\alpha=3.40$  eV/Å<sup>3</sup>. The downward arrows show the location, from left to right, of the metastable minimum  $u_{ms}=0$ , maximum, and the stable minimum  $u_s$ , of the on-site potential (Fig. 1). (a) Three temperatures in the “cooling” series. (b) Three temperatures in the “heating” series.

TABLE IV. Kurtosis (ratio of the fourth moment to the square of the second moment) of position probability distribution. All data are for heating. The entry  $T_1$  indicates where the transition occurs for each  $\alpha$ .

		$\alpha$ (eV/Å <sup>3</sup> )					
1.50		2.00		3.40			
$T$ (K)	Kurtosis	$T$ (K)	Kurtosis	$T$ (K)	Kurtosis		
199.4	3.09	949.7	3.53	199.3	3.06		
299.4	3.13	999.5	3.62	299.4	3.10		
399.4	3.21	1048.5	3.82	399.4	3.15		
499.4	3.26	1059.4	3.99	499.4	3.20		
599.4	3.28	1065.1	4.03	599.4	3.24		
699.5	3.31	1067.8	4.05	699.8	3.33		
799.6	3.40	1068.2	3.91	799.2	3.38		
900.7	3.46	$T_1$		898.3	3.50		
1000.0	3.51	1071.6	2.86	930.3	3.56		
1096.1	3.58	1074.7	2.85	933.7	3.56		
1199.9	3.02	1099.4	2.86	934.8	3.56		
$T_1$		1200.5	2.83	936.8	3.56		
1203.8	2.93			$T_1$			
1209.6	2.63			937.0	2.89		
1211.2	2.57			939.3	2.89		
1224.2	2.47			998.9	2.88		
1299.4	2.63			1099.2	2.97		
1399.9	2.66			1199.0	2.87		

which are extremely narrow on linear plots.

The spectral functions in Fig. 16(a) for  $T=199.27$  K show three important features: (1) a strong phonon peak; (2) a much weaker quasielastic maximum or “central peak” with a sharp cutoff; and (3) high-frequency structure. The position of the phonon peak and the cutoff on the central peak move with  $q_x$ ; these dispersion relations

are given below. The position of the high-frequency structure is independent of  $q_x$  at about  $\omega/\omega_0 \approx 1.2$ , but seems to show complicated interference effects with the phonon part of the spectrum when  $q_x$  becomes large enough for the phonon frequency to move into that part of the spectrum. All of these features remain at the higher temperatures [Figs. 16(b) and 16(c)], but the pho-

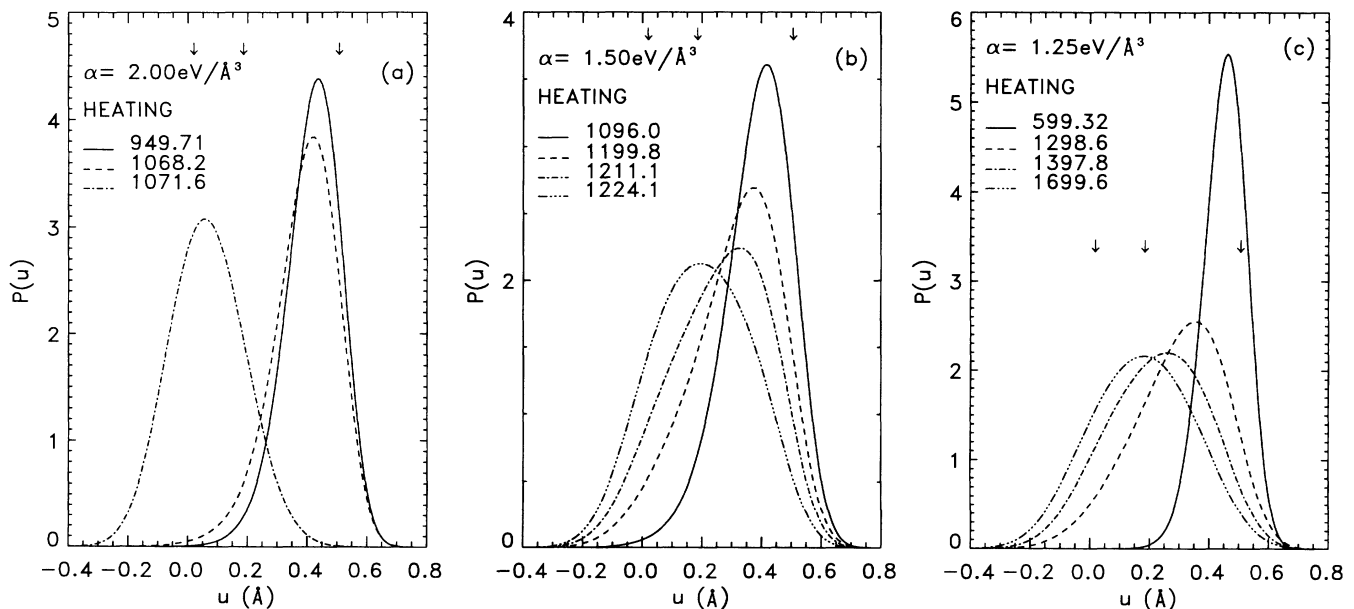


FIG. 15. Position probability distribution at different  $\alpha$  values and temperatures in the “heating” series. The downward arrows show the location of the metastable minimum  $u_{ms}=0$ , maximum, and the stable minimum  $u_s$  of the on-site potential (Fig. 1). (a)  $\alpha=2.00$  eV/Å<sup>3</sup>. The two higher temperatures are just below and just above the transition. (b)  $\alpha=1.50$  eV/Å<sup>3</sup>. (c)  $\alpha=1.25$  eV/Å<sup>3</sup>.

non peaks broaden, the central peak cutoff is not so sharp, and the high-frequency structure in the spectrum is harder to discern, especially at the larger wave vectors.

In Fig. 17 we plot the location of the phonon peaks versus wave vector for  $T < T_1$  (left panel) and  $T > T_1$  (right panel). On both panels, the solid curve is the theoretical phonon dispersion relation for small oscillations in the appropriate well of the on-site potential, i.e., the solid line on the left of Fig. 17 shows (the square root of) Eq. (2.8) for oscillations about the stable minimum, and on the right Eq. (2.9) for small oscillations about the metastable minimum. For  $T$  increasing up to  $T_1$ , the whole phonon spectrum softens with the long-wavelength part decreasing more than the rest of the spectrum. However, this softening is considerably less than that occurring at the second-order transition of the  $\phi^4$  system.<sup>11</sup> At  $T_1$  two effects occur. The first is that the

small wave-vector part of the spectrum “hardens” somewhat, up to the value appropriate for small oscillations in the metastable well [cf. Eqs. (2.8) and (2.9)]. Moreover, for larger wave vectors the slope of  $\omega(q_x, 0)$  decreases considerably. Since most of the particles are now in the metastable well, the anharmonicity introduced in the interparticle interactions through the terms proportional to  $\alpha$  is now essentially absent. The total effect is that the average phonon frequency is lower in the high-temperature phase, even though the part of the spectrum near  $q \approx 0$  increases. Overall, these changes are in agreement with Zener’s discussion of the mechanism for  $\beta$ -cubic–close-packed transitions.<sup>19</sup>

Now we discuss the “central peak” part of the spectrum. The dispersion relation for the cutoff frequency (the downward arrows on the plots in Fig. 16) is graphed in Fig. 18; it is a linear function of the wave vector to

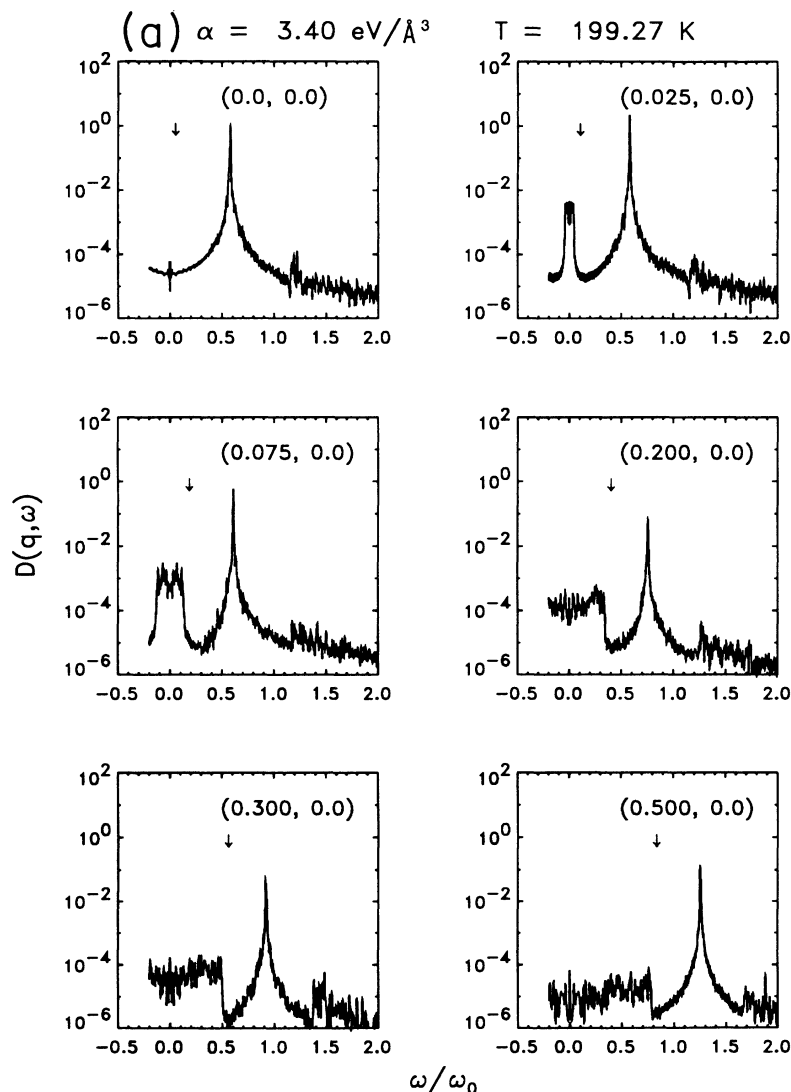


FIG. 16. Spectral function (semilogarithmic plot) for displacement fluctuations at  $\alpha = 3.40 \text{ eV}/\text{\AA}^3$ . The different plots are for different wave vectors  $\mathbf{q}$ ; the components of  $\mathbf{q}$  are written on each plot, expressed as a fraction of the Brillouin-zone boundary ( $q/\pi$ ). The arrows locate the cutoff of the quasielastic part of the spectrum. (a)  $T = 199.27 \text{ K}$ . Notice the high-frequency structure around  $\omega/\omega_0 \approx 1.2$ . (b)  $T = 936.77 \text{ K}$ , just below the transition. (c)  $T = 936.99 \text{ K}$ , just above the transition.

reasonable accuracy. The cutoff frequencies are very temperature *independent* within each phase; for example, the graph for  $T=199.27$  K is nearly identical to the one shown for  $T=936.77$  K. However, there is a definite change in the slope at the transition. The values of these slopes in each temperature range are nearly the same as the slopes of the corresponding phonon dispersion relation in the linear region at the larger  $q_x$  values (see Fig. 17); that is, they are accurately equal to the velocity of "linear" sound that would be obtained by omitting the constant frequency term from the discrete Klein-Gordon equation in Eq. (2.7).

Figure 19 shows the wave-vector dependence of the total and central peak intensity just below the transition. The shapes of the two curves are generally the same at other temperatures. However, the fraction of the intensity in the central peak is maximum at this temperature, being approximately 20% of the total for  $ql/\pi \leq 0.2$  and falling to about 5% of the total for larger wave vectors.

At  $T=199$  K, the fraction in the central peak is reduced by a factor of about 20. Just above the transition at  $T=936.77$  the fraction in the central peak is reduced by about a factor of 3 from its value just below  $T_1$ . If we take the wave vector  $ql/\pi \approx 0.2$ , where the central peak intensity begins to decrease more rapidly than the total intensity, as a measure of the size of the nonlinear fluctuations which contribute to the central peak, then these fluctuations extend over roughly 10 lattice constants.

These properties of the spectral functions are very similar to those which occur in one-dimensional sine-Gordon systems. Computer simulations<sup>31</sup> of that system give a central peak with a sharp cutoff at  $c_0q$ , where  $c_0$  is the velocity of "linear" sound. Ideal-gas phenomenology<sup>32</sup> attributes this central peak to soliton and breather propagation. One would like to make a similar interpretation here, but there are two reservations. The first is that sine-Gordon solitons depend on the existence of degenerate ground states and thereby acquire a *topological*

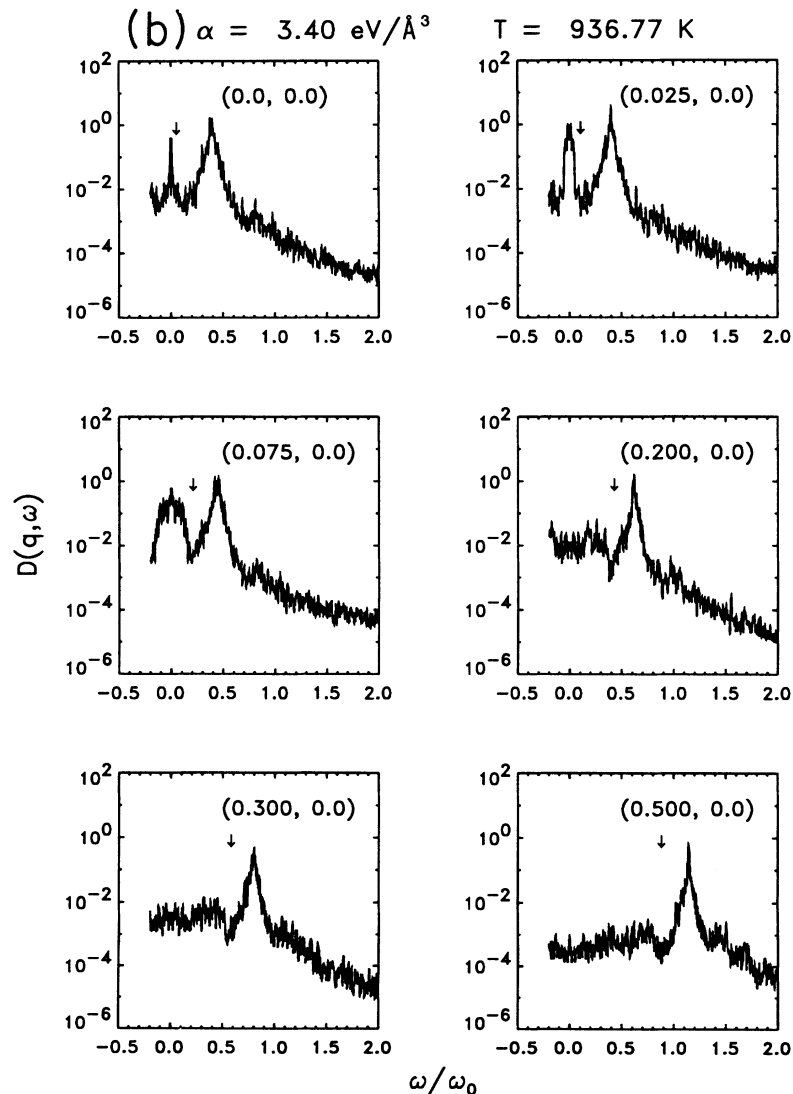


FIG. 16. (Continued).

character. There are no topological solitons for the asymmetric on-site potential. This objection does not apply to breathers, and so one may speculate that breather-type motions are responsible for the central peak seen here. The second reservation is that the system here is two dimensional and very *isotropic* (cf. Fig. 11). Very little is known about propagating nonlinear entities in dimensions greater than one, and so there is no theory on which to base a phenomenological calculation of these spectral functions.

The existence of the high-frequency structure in the spectrum can be interpreted as further evidence showing the existence of breather-type motions. In addition to propagation, breathers have a high-frequency internal oscillation. In the sine-Gordon system this oscillation makes a contribution to the high-frequency part of appropriate spectral functions.<sup>31,32</sup>

### V. DISCUSSION

We have presented the results of a simulation of an apparent first-order phase transition, intended to be a first

approximation to the transformation undergone by Zr, under pressure or upon alloying, from the bcc to the  $\omega$  phase. The major conclusions from these calculations are the following. (1) The thermodynamic functions collected in Figs. 3–13 show that the combination of asymmetry in the on-site potential plus anharmonicity in the interparticle interaction suffices to produce a first-order transition in this system with a one-component order parameter. These thermodynamic functions show the evolution of a latent heat on heating, with a concomitant jump in the order parameter, at a first-order transition temperature  $T_1$ . The change in the system is extremely abrupt, with no appreciable change in the range of the correlations as  $T_1$  is approached from below. (2) The *absence* of two maxima in the position probability distributions in Figs. 14 and 15 for temperatures near the transition shows that the formation of large precursor clusters of the other phase is *not* occurring in this system. (3) The existence and wave-vector dependence of the central peak in the dynamic structure factor (Fig. 16) indicates (by analogy with the sine-Gordon system) that propagating

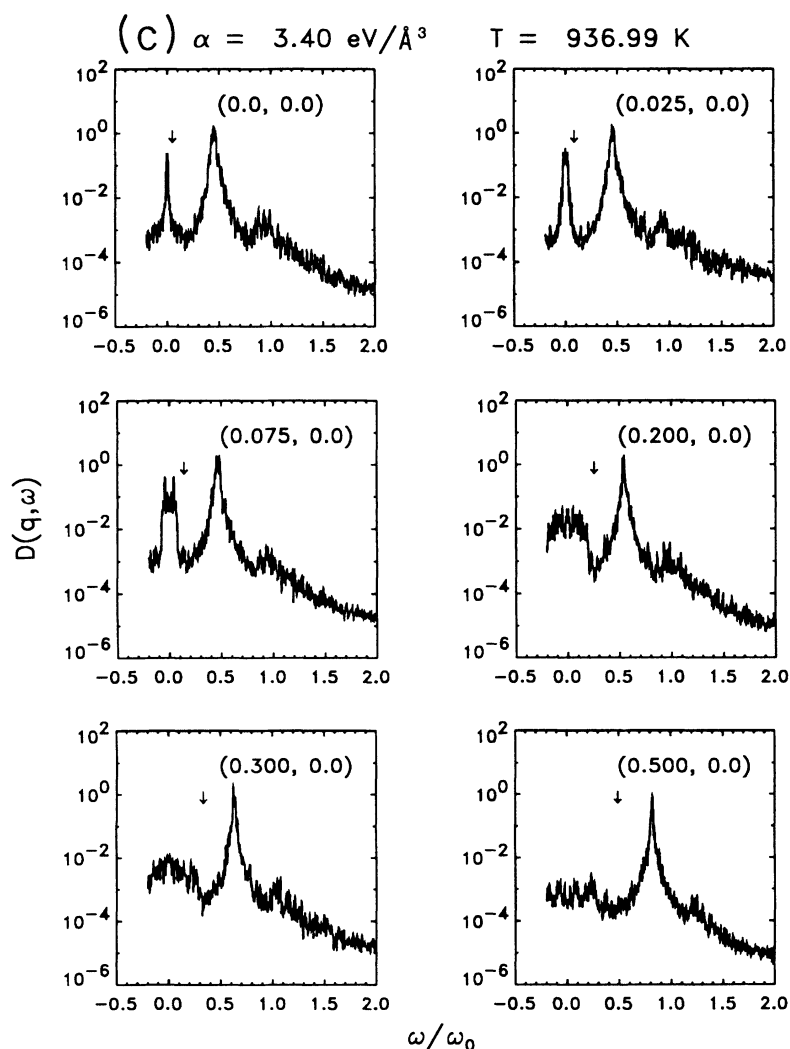


FIG. 16. (Continued).

nonlinear entities exist in this system.

However, several issues remain unresolved, which we review here. First, note in Fig. 1 that the on-site potential is *not* symmetric, viz.,  $V(u) \neq V(-u)$ . Thus, the expectation value of the displacement, which is the order parameter, should never be zero, and this is indeed seen in Figs. 7 and 8. However, in Figs. 3–10 we seem to be observing something which resembles a first-order phase transition. This is not a symmetry-breaking transition, since already the on-site potential (and thus the Hamiltonian) lacks inversion symmetry, so it is interesting to observe so many features that are reminiscent of symmetry-breaking transitions.

Secondly, one feature that stands out in our simulations is the huge hysteresis loop in the case where we did both “cooling” and “heating” runs ( $\alpha = 3.40 \text{ eV/\AA}^3$ ). On cooling, we never observed a transition of the particles out of the metastable minimum of their on-site potentials, even though we followed the system for  $10^{-9}$  sec. On the “heating” series, where the initial conditions at the lowest temperature had all the particles near the stable minimum, a transition of some kind does occur at close to 937 K (for this  $\alpha$  value). An alternative interpretation to this being a first-order transition can be based on the results for specific heat (Fig. 6) and susceptibility (Fig. 9). Those plots could be interpreted as possibly showing a tendency to diverge, as at a second-order transition. Our numerical results are not accurate enough to distinguish between a discontinuity and a divergence. If we assume that they are diverging, then we would say, using the language of mean-field theory,<sup>33</sup> that our observed transition is the limit of metastability of the low-temperature phase, where these thermodynamic functions would behave as we have observed. To be specific, there is a

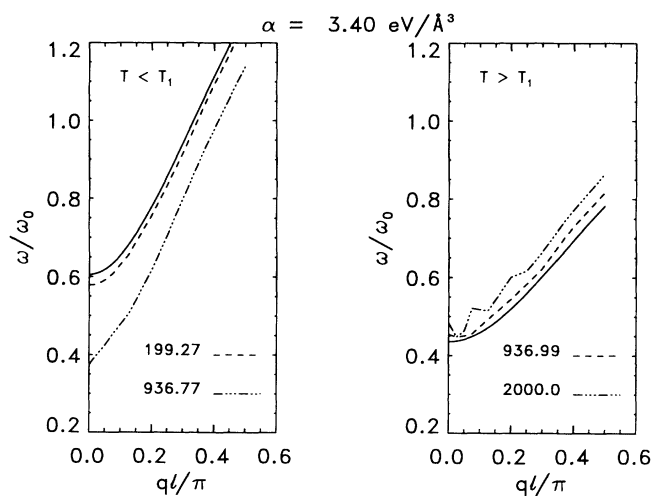


FIG. 17. Dispersion relations for the phonon peak of the spectral functions (previous figures). For the left panel  $T$  is below the transition, and for the right panel it is above. The solid lines are the phonon dispersion relations for the linearized equations of motion. For the left panel, the linearization is about the stable minimum of the on-site potential [Eq. (2.8)], and for the right panel it is about the metastable minimum [Eq. (2.9)].

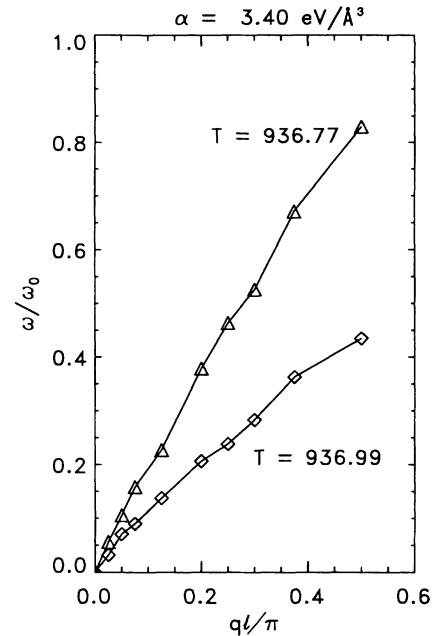


FIG. 18. Location of the cutoff frequency for the quasielastic part of the spectral functions for temperatures just below and just above the transition.

discontinuity in the order parameter and energy, but, in contrast, the specific heat and susceptibility are divergent. The Landau theory of this transition (in the absence of the  $\alpha$  nonlinear intersite interaction) was previously discussed<sup>13</sup> and it was found that the parameter  $A(T)$  in Eq. (1.4) acquired the value of  $\frac{2}{9}$  at the transition (see Fig. 1). Unfortunately, self-consistent phonon theory<sup>13,34</sup> does not allow for a simple consideration of the cubic term in the potential (viz., when only linear variations in the free energy are considered, odd order terms in the Hamiltonian are not accounted for), and thus it is difficult to test the conjecture that this is simply

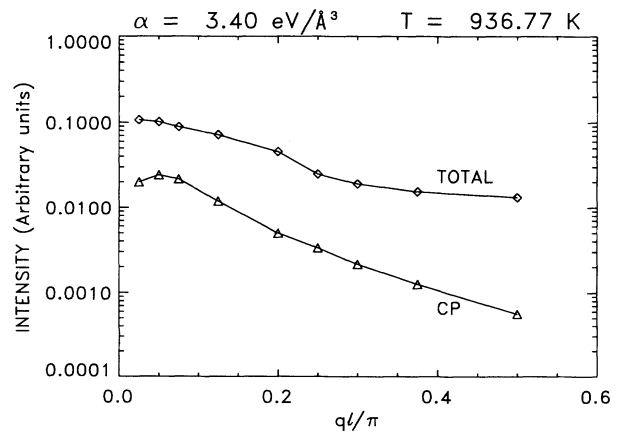


FIG. 19. Wave-vector dependence of the total and central peak intensities of the spectral functions at a temperature just below the transition.

a loss of metastability, and not a first-order phase transition—much more sophisticated variational theories are required.<sup>35</sup>

The resolution to this dilemma follows from Figs. 3 and 4, where the importance of the  $\alpha$  nonlinear intersite coupling term in the Hamiltonian is seen. As discussed extensively in Sec. II (and in Ref. 18 for the symmetry-breaking case), the role of this term is to change the dispersion of the phonons in the two states, which then increases the entropy of the metastable well state in comparison to the stable well state. Then an impetus is provided for an entropy-driven transition.<sup>18</sup> In Fig. 3 we see evidence for such an entropy-driven transition in that a latent heat is clearly evolved for sufficiently large  $\alpha$ . More evidence for this association is provided by the fact that if  $\alpha$  gets too small, we never observe a jump in the internal energy. Thus, the transitions that we observe are indeed below the metastability limit of the stable well phase, and in the parlance of mean-field theory,  $T \approx 937$  K (for  $\alpha = 3.40$  eV/Å<sup>3</sup>) corresponds to somewhere between  $\frac{2}{9}$  and  $\frac{2}{8}$  for the Landau-type parameter  $A(T)$  in Eq. (1.4). Further, the transition is driven by the vibrational entropy difference between parent and product phases produced by the nonlinear, intersite coupling term.

So, at least on heating we have clear evidence of a first-order transition. Thus, we may discuss the primary focus of this study, namely, the dynamics associated with the first-order phase transition. As mentioned above, the probability distribution function clearly shows that in the equilibrium state assumed by the system (on heating) when allowed to evolve for  $10^{-9}$  sec, there is only one maximum, but there is also nonzero probability of the fluctuations tending towards the metastable well from the stable well as  $T$  is increased. This is shown qualitatively from the kurtosis listed in Table IV, where, as the transitions (for different  $\alpha$ ) are approached, the wings of the distribution function grow. This behavior of  $P(u)$  is very different from that displayed by the same function for the case of a symmetry-breaking first-order transition<sup>18</sup> caused by the same mechanism for producing temperature dependent phonons. A major question for further work is to understand the reasons for this difference.

In order to study the dynamics of these fluctuations, one must turn to the dynamic structure factor shown in

Fig. 16. The central peak is clear evidence of the coherent nonlinear nature of these fluctuations, but what is not clear is their amplitude. That is, for these fluctuations to be true heterophase fluctuations (e.g., on the low-temperature side of the transition), they must carry particles away from the stable minimum of the on-site potential, as far as the “spinodal point” (vanishing second derivative) or over the maximum into the metastable well. The analogue of these fluctuations in the sine-Gordon system is *large-amplitude* breathers, which carry particles over the potential maxima into adjacent wells of that periodic potential. To be nonlinear the fluctuations have to move the particles only far enough from the bottom of the well for the anharmonicity to be felt. The analogue of these fluctuations in the sine-Gordon system is *small-amplitude* breathers.

More work will be required to elucidate the issues raised by our simulation. Why does the hysteresis loop on cooling extend down to the lowest temperature studied? How could there possibly be a potential barrier that is accessible on heating, as opposed to cooling? Answers to these questions may be provided when Langevin dynamics simulations are completed. Secondly, and most importantly, what are the nonlinear excitations associated with the central peak that appears in the dynamic structure factor? From graphs of displacement profiles we have found similarities between the evolution of the displacements in these 2D simulations and that found in 1D, from which dynamical motion, e.g., interfacial propagation, may be more easily studied analytically. These results will be presented in a separate paper.<sup>36</sup> Eventually we plan to do simulations using more realistic symmetry restricted anharmonic on-site potentials representative of a wide class of first-order structural phase transitions.<sup>37</sup>

#### ACKNOWLEDGMENTS

The computational resources used for this research were partially supported by NSF Grant No. CHE-8913800 to Wake Forest University. The work of W.C.K. was partially supported by a grant from the Research Corporation, of R.J.G. by NSERC of Canada, of A.R.B. by the US DOE, and JAK by the US DOE. We thank J. Morris for valuable assistance.

\*Present address: Department of Physics, Indiana University, Bloomington, IN.

<sup>1</sup>A. Heiming, W. Petry, J. Trampenau, M. Alba, C. Herzig, and G. Vogl, *Phys. Rev. B* **40**, 11 425 (1989); W. Petry, A. Heiming, J. Trampenau, M. Alba, C. Herzig, H. R. Schober, and G. Vogl, *ibid.* **43**, 10 933 (1991); A. Heiming, W. Petry, J. Trampenau, M. Alba, C. Herzig, H. R. Schober, and G. Vogl, *ibid.* **43**, 10 948 (1991); J. Trampenau, A. Heiming, W. Petry, M. Alba, C. Herzig, W. Miekeley, and H. R. Schober, *ibid.* **43**, 10 963 (1991).

<sup>2</sup>P.-A. Lindgård and O. G. Mouritsen, *Phys. Rev. Lett.* **57**, 2458 (1986).

<sup>3</sup>Z. Nishiyama, *Martensitic Transformations* (Academic, New York, 1978).

<sup>4</sup>A. D. Bruce and R. A. Cowley, *Structural Phase Transitions* (Taylor and Francis, London, 1981). This book is based on three published articles: R. W. Cowley, *Adv. Phys.* **29**, 1 (1980); A. D. Bruce, *ibid.* **29**, 111 (1980); A. D. Bruce and R. A. Cowley, *ibid.* **29**, 219 (1980).

<sup>5</sup>W. Cochran, *Adv. Phys.* **9**, 387 (1960); P. W. Anderson, in *Fizika Dielektrikov*, edited by G. I. Skanov and K. V. Fillippov (Academy of Sciences, Moscow, 1960), p. 290.

<sup>6</sup>R. A. Cowley, *Philos. Mag.* **11**, 673 (1964); *Adv. Phys.* **12**, 421 (1964).

- <sup>7</sup>A. A. Maradudin and A. E. Fein, *Phys. Rev.* **128**, 2589 (1962).
- <sup>8</sup>K. A. Müller, in *Statics and Dynamics of Nonlinear Systems*, edited by G. Benedek, H. Bilz, and R. Zeyher, Springer Series in Solid State Sciences Vol. 47 (Springer, Berlin, 1983) p. 68.
- <sup>9</sup>J. A. Krumhansl and J. R. Schrieffer, *Phys. Rev. B* **11**, 3535 (1975); S. Aubry, *J. Chem. Phys.* **62**, 3217 (1975); **64**, 3392 (1976); A. R. Bishop and J. A. Krumhansl, *Phys. Rev. B* **12**, 2824 (1975).
- <sup>10</sup>T. Schneider and E. Stoll, *Phys. Rev. B* **13**, 1216 (1976); **17**, 1302 (1978).
- <sup>11</sup>W. C. Kerr and A. R. Bishop, *Phys. Rev. B* **34**, 6295 (1986).
- <sup>12</sup>M. Plischke and B. Bergersen, *Equilibrium Statistical Mechanics* (Prentice-Hall, Englewood Cliffs, 1989), p. 74 ff.
- <sup>13</sup>J. A. Krumhansl and R. J. Gooding, *Phys. Rev. B* **39**, 3047 (1989).
- <sup>14</sup>S. M. Shapiro, B. X. Yang, G. Shirane, Y. Noda, and L. E. Tanner, *Phys. Rev. Lett.* **62**, 1298 (1989) on  $\text{Ni}_{62.5}\text{Al}_{37.5}$  finds  $T_0 \approx -30$  K while  $T_{\text{trans}} \approx 85$  K. Also from Ref. 1, the  $\beta \rightarrow \alpha$   $N$ -point phonon data for Ti and Zr indicate  $T_0 < 100$  K while  $T_{\text{trans}} \approx 882^\circ\text{C}$  and  $865^\circ\text{C}$ , respectively.
- <sup>15</sup>H. E. Cook, *Acta Metall.* **23**, 1027 (1975); **23**, 1041 (1975).
- <sup>16</sup>Background discussion can be found in J. A. Krumhansl, in *Competing Interactions and Microstructures: Statics and Dynamics*, edited by R. LeSar, A. R. Bishop and R. Heffner, Springer Proceedings in Physics Vol. 27 (Springer, Berlin, 1988), p. 50.
- <sup>17</sup>K. M. Ho, C. L. Fu, and B. N. Harmon, *Phys. Rev. B* **29**, 1575 (1984). The  $\frac{2}{3}(1,1,1)$  LA phonon in Zr has quite low (harmonic) frequency. For large displacements the potential energy computed by a frozen phonon method can be approximated by Eq. (2.2) with suitable coefficients. The cubic phase (i.e.,  $u_i = 0$ ) is metastable against static displacement to finite amplitude of that mode; the resulting distortion produces one variant of the hexagonal “ $\omega$  phase.”
- <sup>18</sup>R. J. Gooding, *Scr. Metall.* **25**, 105 (1991); J. R. Morris and R. J. Gooding, *Phys. Rev. Lett.* **65**, 1769 (1990); *Phys. Rev. B* **43**, 6057 (1991).
- <sup>19</sup>C. Zener, *Phys. Rev.* **71**, 846 (1947).
- <sup>20</sup>Y. Y. Ye, K.-M. Ho, B. N. Harmon, and P. A. Lindgård, *Phys. Rev. Lett.* **58**, 1769 (1987); F. Willaime and C. Massobrio, *ibid.* **63**, 2244 (1989). These papers discuss the phonon and electronic entropy contributions to the  $\beta \rightarrow \alpha$  transition.
- <sup>21</sup>R. A. Cowley and A. D. Bruce, *J. Phys. C* **11**, 3577 (1978); A. D. Bruce, R. A. Cowley, and A. F. Murray, *ibid.* **11**, 3591 (1978); A. D. Bruce and R. A. Cowley, *ibid.* **11**, 3609 (1978).
- <sup>22</sup>P. Chandra, *Phys. Rev. A* **39**, 3672 (1989); T. Ohta, *J. Phys.: Condens. Matter* **2**, 9685 (1990); S. Marais, V. Heine, C. Nex, and E. Salje, *Phys. Rev. Lett.* **66**, 2480 (1991).
- <sup>23</sup>For example, J. Callaway, *Quantum Theory of the Solid State* (Academic, New York, 1974), p. 25.
- <sup>24</sup>This staggered structure was initially found in simulations at  $\alpha = 6.80 \text{ eV}/\text{\AA}^3$ . The run was initialized in a spatially uniform structure at low temperature, which is, in fact, metastable at this  $\alpha$  value, and made a transition to the staggered structure at higher temperature. The transition exhibited some bizarre “thermodynamic” features, e.g., a negative latent heat.
- <sup>25</sup>D. Beeman, *J. Comput. Phys.* **20**, 130 (1976).
- <sup>26</sup>K.-M. Ho, C. L. Fu, and B. N. Harmon, *Phys. Rev. B* **29**, 1575 (1984).
- <sup>27</sup>J. Morris (private communication).
- <sup>28</sup>C. Stassis, J. Zaretsky, and N. Wakabayashi, *Phys. Rev. Lett.* **41**, 1726 (1978).
- <sup>29</sup>J. L. Lebowitz, J. K. Percus, and L. Verlet, *Phys. Rev.* **153**, 250 (1967).
- <sup>30</sup>For example, G. H. Wannier, *Statistical Physics* (Wiley, New York, 1966), p. 479.
- <sup>31</sup>W. C. Kerr, D. Baeriswyl, and A. R. Bishop, *Phys. Rev. B* **24**, 6566 (1981); W. C. Kerr, A. R. Bishop, and S. N. Kerr, in *Nonlinearity with Disorder*, edited by F. Kh. Abdullaev and A. R. Bishop, Springer Proceedings in Physics (Springer, Berlin, to be published).
- <sup>32</sup>A. R. Bishop, *J. Phys. A* **14**, 1417 (1981).
- <sup>33</sup>K. Binder, *Rep. Prog. Phys.* **50**, 783 (1987).
- <sup>34</sup>N. Boccara and G. Sarma, *Physics* **1**, 219 (1965).
- <sup>35</sup>J. R. Morris and R. J. Gooding (unpublished).
- <sup>36</sup>W. C. Kerr, A. M. Hawthorne, D. A. Waldron, R. J. Gooding, A. R. Bishop, and J. A. Krumhansl (unpublished).
- <sup>37</sup>R. J. Gooding, *Mater. Sci. Eng. A* **127**, 183 (1990).